

Simultaneously Enhancing Radiation and Aperture Efficiencies of Leaky Wave Antennas Using Discrete Metasurfaces

Chu Qi and Alex M. H. Wong, *Senior Member, IEEE*

Abstract—Traditional leaky wave antennas (LWAs) designed with remaining power absorbed at the end of the waveguide leads either to poor radiation efficiency or to poor aperture efficiency. In this work, we propose a novel class of LWAs based on discrete metasurfaces. A reflector is placed at the waveguide end to reflect and reuse the remaining power. A novel discrete metasurface is designed to radiate the power leaked from the forward and backward-travelling waves to the same direction. The antenna termination is tuned to realize a constructive interference between the waves leaked from the forward and backward-travelling waves. Moreover, the metasurface can be designed to control the leakage factor and the radiation direction. To verify the concept, two LWAs are designed to realize broadside radiation and 31° tilted radiation respectively. Compared to the same LWAs terminated with a matched load, the proposed LWAs achieve gain enhancements of 3.5 dB and 2.0 dB respectively. The proposed LWAs are fabricated and measured, the experimental results agree well with the simulated results. The proposed concept can be used to design LWAs with improved radiation efficiencies and reduced antenna lengths, which can find potential applications in various communication systems.

Index Terms – Discrete metasurface, leaky wave antenna, gain enhancement.

I. INTRODUCTION

THE leaky wave antenna (LWA) has been attracting increasing research interest due to its simple feeding structure, high directivity, and beam scanning capability. It is based on a waveguiding structure which gradually radiates power while the guided wave propagates along it. The LWA's radiation characteristics are intrinsically determined by the complex propagation wavenumber of the leaky mode, whose phase constant determines the radiation direction, and the leakage factor determines the directivity [1-4]. By independently controlling the phase and leakage factors, the LWA can be designed to realize versatile radiation patterns.

This work was supported by the Research Grants Council of the Government of Hong Kong through grants C6012-20 GF and AoE/E-101/23-N. (Corresponding author: Alex M. H. Wong.)

Chu Qi is with the Department of Physics and Electronic Engineering, Sichuan Normal University, Chengdu, China and the Department of Electrical Engineering, City University of Hong Kong, Hong Kong. (e-mail: chuqi2@um.cityu.edu.hk).

Alex M. H. Wong is with the State Key laboratory of Terahertz and Millimeter Waves, Department of Electrical Engineering, City University of Hong Kong, Hong Kong. (e-mail: alex.mh.wong@cityu.edu.hk).

In traditional LWA designs, the nonradiated power is usually absorbed by a matched load placed at the end of the waveguide, leading to poor radiation efficiencies. For an LWA based on slotted-waveguide array [5], an increased radiation efficiency can be realized by terminating the waveguide with a short end (thus generating a resonant standing wave inside the waveguide) and locate the slots at the standing wave peaks. However, the resonant slot-waveguide arrays can only realize broadside radiation [6]. Ref. [7] proposes a power-recycling feeding network to increase the radiation efficiency of a two-dimensional LWA array. In a subsequent work [8], the same group proposes a power-recycling feedback system which feeds back the nonradiated power to the input of an LWA. While this can increase the radiation power of an LWA with reduced length, the power-recycle feedback system is very sensitive to the working frequency, leading to a very narrow band (about 2%) performance. Generally, a high radiation efficiency can be realized by increasing the LWA length. For LWAs with typical values of leakage factors, a radiation efficiency of 90% usually requires a waveguide length of about 10 free space wavelengths, which may be impractical for applications requiring a more compact size. Moreover, the extremely low absolute power leakage near the waveguide end will lead to poor aperture efficiency and poor sidelobe behavior. Therefore, in conventional LWA designs, there is always a compromise between the radiation efficiency and the antenna length.

Recently, researchers have investigated many methods to tailor the radiation pattern of the LWA. Some researchers optimize an LWA to achieve a desired radiation performance [9-11]. Ref. [9] optimizes the phase and leakage factor distributions along the antenna to realize prescribed aperture fields. In [10], the authors minimize the beamwidth or maximize the gain by optimizing the antenna length (with a fixed leakage factor) or the leakage factor (with a fixed antenna length). In a subsequent work [11], the same group uses a partially reflecting surface in the LWA design, and maximizes the gain by optimizing the surface impedance and the waveguide height. The emergence of metasurfaces enables advanced manipulation of electromagnetic (EM) waves by controlling their phase, amplitude, and polarization with a planar structure [12, 13]. Therefore, metasurfaces have been widely used in LWA designs [14-22]. For example, LWAs based on modulated metasurfaces can couple surface waves to propagating waves (leaky waves) by modulating the surface impedance or reactance [15-21]. Based on this, researchers

propose aperture field synthesis in LWA designs by synthesizing desired radiation patterns using modulated metasurfaces [16-18]. More recently, Huygens' metasurfaces have been proposed to provide full control of reflected and transmitted waves [23, 24]. LWAs based on Huygens' metasurfaces are designed to achieve controlled radiation with arbitrary radiation direction and leakage factor [25-30]. In [30], the authors realize the control of LWA aperture field distribution using a bianisotropic Huygens' metasurface, which is designed to realize a gradually changing leakage factor along the antenna length. Moreover, there are also studies on the LWAs based on reconfigurable metasurfaces to realize more advanced applications [31-33]. However, all these works report wave shaping and radiation generation from a wave that travels from the feed location to the termination location within the waveguide. To avoid spurious radiation, the wave that propagates to the end of the waveguide is absorbed. This leads to limited aperture efficiencies.

We propose a solution to this problem using an aggressively discretized metasurface [34-39], which is a kind of metagrating [40-44]. The aggressively discretized metasurface is realized by designing the metasurface with the least number of elements required to realize sufficient control of the propagating diffraction modes, thus achieving the advantages of simplicity and high efficiency. In previous works, we have shown that aggressive discretization in a metasurface design can lead to an interesting functionality of diffraction mode circulation [34], where the metasurface may contribute strongly differing transverse momenta to incident waves from different directions. This contributes a new possibility in designing metasurface-enabled antennas, including LWAs.

In this work, we propose LWAs based on discrete metasurfaces. Different from a traditional LWA with remaining power absorbed at the end of the waveguide, we terminate the waveguide with a perfect electric conductor (PEC) to reflect the remaining power. An aggressively discretized metasurface is designed to redirect the leaked power from the forward and backward-travelling waves to the *same radiation direction*. A constructive interference between the waves leaked from the forward and backward-travelling waves is realized by tuning the antenna termination. Therefore, our proposed LWAs can realize high radiation efficiencies with relatively short antenna lengths. Moreover, by designing the discrete metasurface, the proposed LWAs can realize independent control of leakage factor and radiation direction. As examples, we design two LWAs with different radiation directions. Firstly, an LWA based on a two-element discrete metasurface is designed to realize broadside radiation. Secondly, an LWA based on a six-element discrete metasurface is designed to realize a 31° tilted radiation. We show the radiation efficiency improvement by comparing the maximum realized gain of our proposed LWA to that of the same LWA but terminated with a matched load. Full-wave simulations and experimental demonstrations agree well with one-another, and show that the LWAs with broadside radiation and tilted radiation can achieve gain enhancements of 3.5 dB and 2.0 dB respectively in simulation, and 4.2 dB and 1.9 dB respectively in experiment.

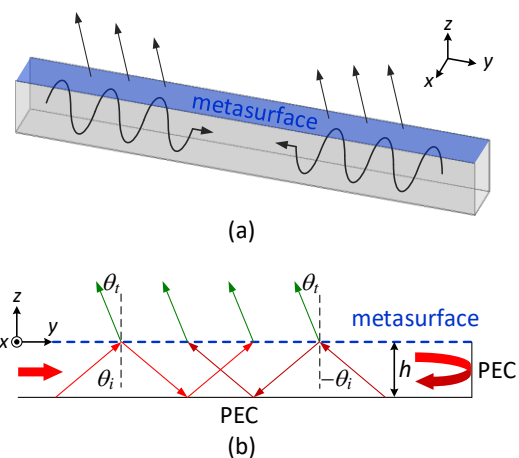


Fig. 1. (a) Working mechanism of the metasurface which radiates forward and backward-travelling waves in the waveguide to the same direction. (b) Working mechanism of the proposed LWA, which is constructed by a rectangular waveguide with a PEC termination and a metasurface in Fig. 1(a).

The rest of this manuscript is organized as follows. Section II introduces the concept and design formulation. Section III details the design and simulation results of the proposed LWAs. Section IV presents the fabrication and experimental results. Section V discusses the bandwidth performance of the proposed LWAs. Section VI concludes this work.

II. CONCEPT AND DESIGN FORMULATION

In this section, we report the concept and design formulation of the proposed LWA. Firstly, we describe the working mechanism of the proposed LWA. Then, we introduce the discrete metasurface design formulation. Lastly, we report the design formulation of the proposed LWA.

A. Working Mechanism of The Proposed LWA

The schematic diagrams in Fig. 1 show the working mechanism of the proposed LWA. The realization of the proposed LWA is based on a discrete metasurface which can radiate the leaked power from the forward and backward-travelling waves in a waveguide to the same direction, as schematically shown in Fig. 1(a). The discrete metasurface transmits a small part of the incident wave and reflects most of the wave with a 180° reflection phase, similar to the metallic waveguide wall it replaces. Therefore, the travelling wave inside the waveguide remains similar when the waveguide wall is replaced by the metasurface. Fig. 1(b) shows a schematic diagram of the proposed LWA. The waveguide is terminated with a PEC to reflect the power which propagates to the end of the waveguide. The waveguide length is along the y-direction. For a wave travelling along +y-direction in an air-filled waveguide, the incident angle θ_i can be found using the transverse resonance condition [45]

$$2hk_0 \cos \theta_i - \pi + \varphi_{r,MS} = 2n\pi, \quad (1)$$

where h is the height of the waveguide, k_0 is the free space wave number, and $\varphi_{r,MS}$ is the reflection phase contributed by

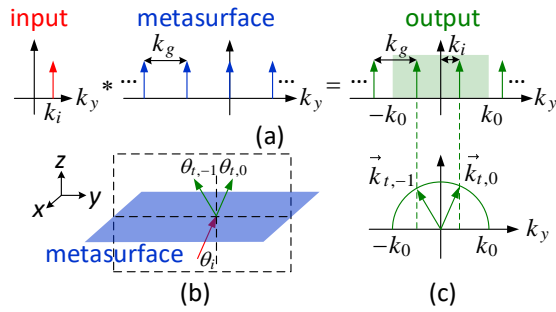


Fig. 2. (a) k -space operation of a periodic metasurface varying along the y -direction. Arrows denote the existence of diffraction modes with different tangential wave numbers. The asterisk sign (*) denotes the convolution operation. The green box in the output spectrum denotes the propagation range of $k_y \in [-k_0, k_0]$ in the free space. (b) Schematic diagram of a transmissive metasurface upon an incidence with an incident angle θ_i and tangential wave number $k_i = k_0 \sin \theta_i$. (c) A diagram showing the correspondence of the output spectrum in Fig. 2(a) to the transmitted wave directions in Fig. 2(b).

the metasurface. Considering the first order ($n = 1$), the incident angle can be expressed as

$$\theta_i = \cos^{-1} \left(\frac{3\pi - \varphi_{r,MS}}{2hk_0} \right). \quad (2)$$

For the guided wave propagating along $-y$ -direction, the incident angle is $-\theta_i$.

Therefore, to radiate the forward and backward-travelling waves in the waveguide to the same direction of θ_t , the metasurface should (i) partially refract the incident waves from θ_i and $-\theta_i$ to the same direction θ_t , and (ii) partially reflect the incident waves from $\pm\theta_i$ to the specular direction. Besides, to achieve the highest gain for the LWA, the waves leaked from the forward and backward-travelling waves should be in phase, resulting in constructive interference. This is realized by tuning the location of the waveguide termination.

B. Discrete Metasurface Design Formulation

The scattering of a discrete metasurface can be investigated by studying its k -space spectrum. A metasurface can be treated as an array of equi-spaced scatterers with similar scattering patterns. Using Fourier transform theory, one can obtain the scattered wave contents (in the spectral domain) generated by the discrete scatterers (in the spatial domain). Conversely, a desired transmission and/or reflection spectrum can be used to find the required transmission and/or reflection coefficients of the metasurface elements [34, 36]. As guaranteed by Fourier transform theory, a metasurface which is periodic and discrete in the spatial domain will have a spectrum which is discrete and periodic in the spectral domain. Fig. 2(a) shows the k -space operation of a periodic metasurface illuminated by a plane wave with an incident angle θ_i and a tangential wave number $k_i = k_0 \sin \theta_i$. The metasurface varies along y -direction with a period Λ_g , therefore its k -space is discrete with an interval $k_g = 2\pi/\Lambda_g$. The arrows denote the existence of diffraction modes with different tangential wave numbers. The output spectrum can be determined by the input and metasurface spectra, with

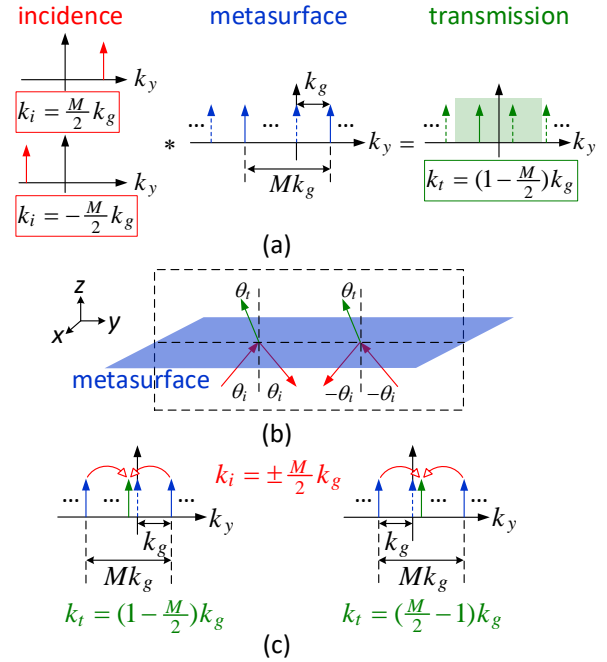


Fig. 3. (a) k -space operation of a metasurface realizing the same transmission spectrum upon different incidences from θ_i and $-\theta_i$. Arrows with solid line denote refraction modes with non-zero magnitude, while arrows with dashed line denote refraction modes with zero magnitude. (b) Schematic diagram of the proposed metasurface. (c) k -space operation of metasurfaces realizing negative and positive θ_t .

the n^{th} mode having a tangential wave number $k_i + nk_g$. In the output spectrum, the diffraction modes within the propagation range ($k_y \in [-k_0, k_0]$) can scatter into the far field, while the other diffraction modes are evanescent. Fig. 2(b) shows the schematic diagram of a transmissive metasurface in Fig. 2(a), the corresponding transmitted wave directions are shown in Fig. 2(c). The angle of the n^{th} transmitted mode is

$$\theta_{t,n} = \sin^{-1} \left(\frac{k_i + nk_g}{k_0} \right). \quad (3)$$

We have shown in [34] that a periodic metasurface with M elements per period will have a metasurface spectrum which is periodic of M diffraction modes. These M diffraction modes can be controlled by the transmission/reflection coefficients of the M metasurface elements. Moreover, different transmitted and reflected wave components can be realized by designing the metasurface to have different transmission and reflection spectra.

For the metasurface required in the LWA, the specular reflection can be easily realized with a uniform reflection coefficient distribution. We design the metasurface transmission coefficient distribution to realize a same transmitted wave direction upon incidences from θ_i and $-\theta_i$. Fig. 3(a) shows the k -space operation corresponding to the required transmission characteristics of the metasurface, which is realized by a transmission profile with a discretization level of M elements per period. In each period of the metasurface transmission spectrum, there is only one mode with non-zero amplitude among the M modes. As shown in Fig. 3(a), the

metasurface has a non-zero $+1^{\text{st}}$ -order diffraction mode, and it will also have a non-zero $(-M + 1)^{\text{th}}$ mode due to the k -space periodicity. For this metasurface, upon incidences with tangential wave numbers of $k_i = \frac{M}{2}k_g$ and $k_i = -\frac{M}{2}k_g$, the output transmission spectrum will have a same non-zero diffraction mode with a tangential wave number of $k_t = (-M + 1)k_g + \frac{M}{2}k_g = k_g - \frac{M}{2}k_g = \left(1 - \frac{M}{2}\right)k_g$. In other words, upon incidences from θ_i and $-\theta_i$, the metasurface can refract the transmitted waves to the same direction θ_t . Using $k_i = k_0 \sin \theta_i$ and $k_t = k_0 \sin \theta_t$, the angles of the incident and transmitted waves can be calculated using

$$\theta_i = \sin^{-1}\left(\frac{M}{2} \frac{k_g}{k_0}\right), \theta_t = \sin^{-1}\left(\left(1 - \frac{M}{2}\right) \frac{k_g}{k_0}\right). \quad (4)$$

Fig. 3(b) shows a schematic diagram showing the transmission and reflection properties of the proposed metasurface.

We now investigate the achievable radiation direction of the LWA using the proposed discrete metasurface. Firstly, the incidences and transmitted diffraction modes should lie within the propagation range, that is

$$\begin{aligned} 0 &\leq |k_i| = k_0 |\sin \theta_i| < k_0, \\ 0 &\leq |k_t| = k_0 |\sin \theta_t| < k_0. \end{aligned} \quad (5)$$

Secondly, to ensure a directive radiation to the desired direction, the designed non-zero transmitted mode should be the only non-zero mode in the propagation range of the transmission spectrum. To satisfy this condition, the most adjacent non-zero diffraction modes should fall out of the propagation range. Due to the k -space periodicity, the most adjacent non-zero diffraction modes are the $(1 + M)^{\text{th}}$ and $(-2M + 1)^{\text{th}}$ modes. Then we can write the condition

$$\begin{aligned} \left|(1 + M)k_g - \frac{M}{2}k_g\right| &> k_0, \\ \left|(-2M + 1)k_g + \frac{M}{2}k_g\right| &> k_0. \end{aligned} \quad (6)$$

Combining (4) – (6) we have

$$\begin{cases} \frac{M}{2 + M}k_0 < k_i \leq k_0, & M \geq 2, \\ \frac{2 - M}{M}k_0 < k_t < \frac{2 - M}{2 + M}k_0, & M \geq 3. \end{cases} \quad (7)$$

Then we can obtain the achievable radiation angle

$$\begin{cases} \theta_t = 0, & M = 2 \\ \sin^{-1}\left(\frac{2 - M}{M}\right) < \theta_t < \sin^{-1}\left(\frac{2 - M}{2 + M}\right), & M \geq 3. \end{cases} \quad (8)$$

From (8), we can see that an LWA based on a two-element metasurface can realize broadside radiation. Based on

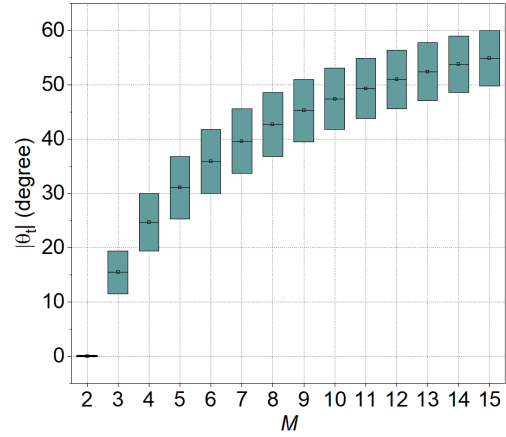


Fig. 4. Achievable radiation angle ranges as a function of the metasurface discretization level M .

metasurfaces with a discretization level of $M \geq 3$, we can design LWAs realizing tilted radiation. We note that from (8), the achievable θ_t is negative. Similarly, a positive θ_t can be realized with an M -element metasurface with a non-zero -1^{st} -order diffraction mode, as shown in Fig. 3(c). Notably, the two scenarios can be achieved with the same metasurface by rotating it by 180° around z -axis. That is, the achievable radiation angle of the proposed LWA is

$$\begin{cases} \theta_t = 0, & M = 2 \\ \sin^{-1}\left(\frac{M - 2}{M + 2}\right) < |\theta_t| < \sin^{-1}\left(\frac{M - 2}{M}\right), & M \geq 3. \end{cases} \quad (9)$$

Fig. 4 plots the absolute values of the achievable radiation angle ranges with $2 \leq M \leq 15$. We observe that the angle range of $0^\circ < |\theta_t| < 11.5^\circ$ can not be realized using the proposed design. By increasing M , the largest achievable radiation angle increases. Since

$$\lim_{M \rightarrow \infty} \left| \sin^{-1}\left(\frac{2 - M}{M}\right) \right| = 90^\circ, \quad (10)$$

we conclude that there is no theoretical limit on the largest achievable radiation angle. However, we remark that an increasing M will also increase the complexity of the metasurface design.

C. LWA Design Formulation

The general design formulation of the proposed LWA with a given radiation angle θ_t is as follows.

1) Discrete metasurface design

With a given radiation angle θ_t , choose the metasurface discretization level M according to Fig. 4. For the broadside radiation with $\theta_t = 0$, the LWA requires a metasurface with $M = 2$. The metasurface wave number can be found using the first equation of (4), namely $k_g = k_0 \sin \theta_i$. Using (7) we can obtain the required incidence range of $\frac{1}{2}k_0 < k_i < k_0$, corresponding to an incident angle of larger than 30° . With the

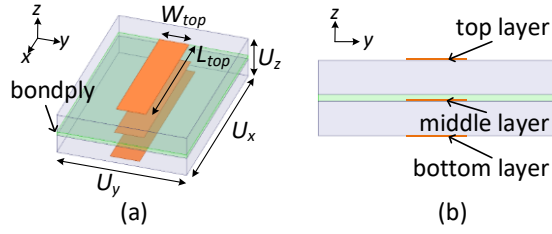


Fig. 5. (a) Perspective view and (b) Front view of the unit cell geometrical structure. The size of the unit cell is $U_x = 5$ mm, $U_y = 3.5$ mm, $U_z = 1.12$ mm.

chosen incidence angle, the metasurface period can be expressed as

$$\Lambda_g = \frac{2\pi}{k_g} = \frac{\lambda_0}{\sin \theta_i}. \quad (11)$$

Then the element size along the varying direction (y-direction) can be calculated using

$$U_y = \frac{\Lambda_g}{M} = \frac{\lambda_0}{M \sin \theta_i} = \frac{\lambda_0}{2 \sin \theta_i}. \quad (12)$$

For tilted radiation with $\theta_t \neq 0$, the LWA requires a metasurface with $M \geq 3$. The metasurface wave number can be found using the second equation of (4), namely $k_g = \frac{2}{M-2} k_0 \sin|\theta_t|$. Then the required incident angle can be determined using the first equation of (4), which is

$$\theta_i = \sin^{-1} \left(\frac{M}{M-2} \sin|\theta_t| \right). \quad (13)$$

Using the determined k_g , the metasurface period can be expressed as

$$\Lambda_g = \frac{2\pi}{k_g} = \frac{(M-2)\lambda_0}{2 \sin|\theta_t|}. \quad (14)$$

The corresponding element size along the varying direction (y-direction) is

$$U_y = \frac{\Lambda_g}{M} = \frac{(M-2)\lambda_0}{2M \sin|\theta_t|}. \quad (15)$$

With element size determined, design the metasurface elements with required reflection and transmission coefficients to realize the desired functionality. To be specific, to realize specular reflection, the metasurface elements should have uniform reflection coefficients. To realize a transmission spectrum as shown in Fig. 3(a), the metasurface transmission coefficients should have the same magnitude and a gradient phase distribution with a phase gradient of $2\pi/M$ radians per element [34].

2) Rectangular waveguide design

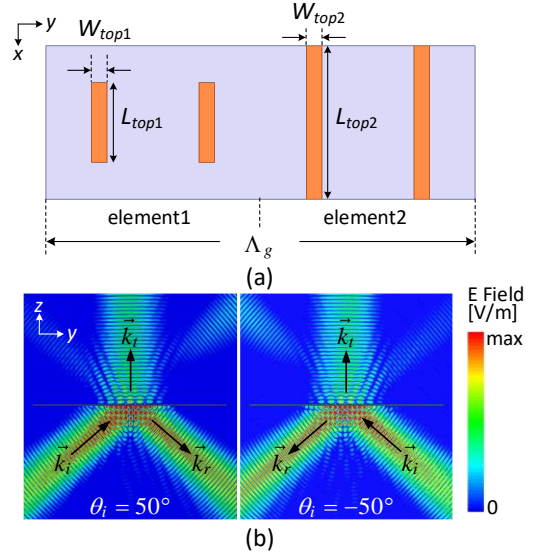


Fig. 6. (a) Top view of one period of the proposed two-element metasurface. (b) The electric field magnitude distributions of the two-element metasurface upon incident Gaussian beams with incident angles of 50° and -50° respectively.

Designing the rectangular waveguide entails finding the waveguide height h , which can be straightforwardly accomplished using (2).

3) LWA design

The proposed LWA is constructed by replacing the top surface of the rectangular waveguide with the discrete metasurface and placing a PEC at the waveguide end. The antenna termination is tuned to realize a constructive interference between the waves leaked from the forward and backward-travelling waves. A high radiation efficiency is realized by designing the LWA with a small reflection coefficient, and hence a high radiated power.

III. LEAKY WAVE ANTENNA DESIGN EXAMPLES

In this section, we introduce the design of two LWAs. Firstly, an LWA is designed to realize broadside radiation with $\theta_t = 0^\circ$. Secondly, an LWA is designed to realize tilted radiation with $\theta_t = 31^\circ$. For the LWA design examples, we consider TE-polarized radiation ($E_y = E_z = H_x = 0$) realized by placing the metasurface as a narrow wall of the rectangular waveguide with TE mode propagating inside it. The TM-polarized radiation ($E_x = H_y = H_z = 0$) can also be realized by using a polarization conversion metasurface. Both LWAs are designed at 28 GHz. The software Ansys HFSS is used for the simulation.

A. Broadside Radiation

A two-element metasurface ($M = 2$) is required in the proposed LWA to achieve broadside radiation. We choose an incidence angle of $\theta_i = 50^\circ$ in this design. Using (12), the required metasurface element size in y-direction is calculated to be 7 mm at the design frequency of 28 GHz. Since the element size is larger than $0.5\lambda_0$, we design the metasurface unit cells with a size of 3.5 mm in y-direction. That means, each metasurface period will have two elements, and each element is

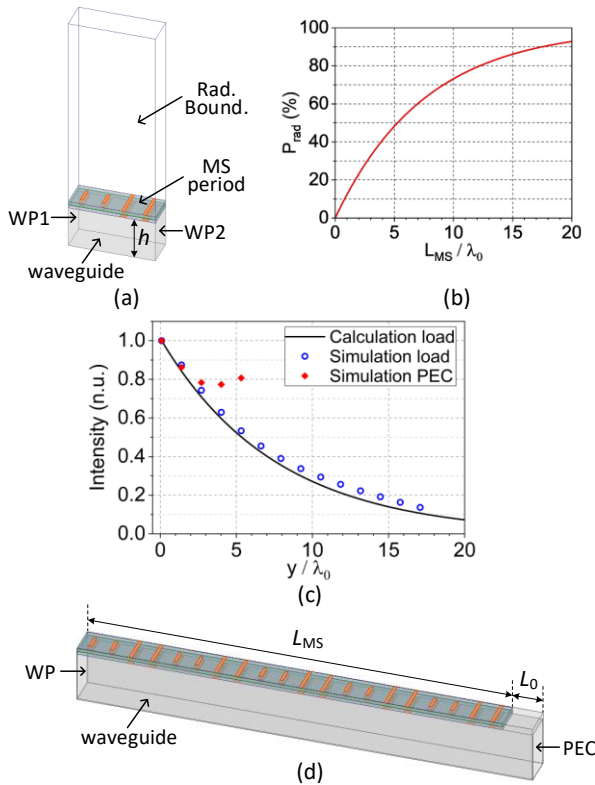


Fig. 7. (a) One period of the LWA realizing broadside radiation. (b) Radiated power as a function of the antenna length, for the LWA terminated with a matched load. (c) Electrical field intensity distribution in the waveguide of the LWAs. (d) Perspective view of the proposed LWA realizing broadside radiation.

composed of two identical unit cells. The metasurface configuration of having multiple identical unit cells in one element has been proposed and validated in a previous work [39].

Fig. 5 shows the geometrical structure of the unit cell, which is constructed using three metallic rectangular strips. We have shown in our previous works [34, 46] that this Huygens' unit cell structure features a simple geometry with broad reflection and transmission phase coverages and a wide-angle response. The structure is designed on two Rogers RO4003C boards ($\epsilon_r = 3.55$, $\delta_t = 0.0027$, thickness: 0.508 mm, copper cladding thickness: 17.8 μm) bonded by a Rogers RO4450F bondply ($\epsilon_r = 3.52$, $\delta_t = 0.004$, thickness: 0.102 mm). The incident and scattered electric fields are along the x-direction. The transmission and reflection coefficients can be varied by tuning the dimensions of the rectangular strip on each layer. By sweeping the widths and lengths of the three rectangular strips, we can tune the amplitudes and phases of the transmission and reflection coefficients of the unit cell with great flexibility. After we establish the library of unit cells, we choose the unit cells with required transmission and reflection coefficients. To realize anomalous refraction and specular reflection, the required unit cells should have opposite transmission coefficients and the same reflection coefficient [34]. A small transmission magnitude is required for a low leakage factor. The absorption loss, calculated using $1 - |S_{21}|^2 - |S_{11}|^2$, should be minimized in the unit cell design. Table I gives the geometrical parameters and S parameters of the two unit cells

in the proposed design. As we can see, the two unit cells have similar transmission and reflection magnitudes. Their transmission phase difference is close to 180° while the reflection phase difference is very small. Fig. 6(a) shows top view of one period of the proposed metasurface. Periodic simulation shows that, upon incidences with $\theta_i = 50^\circ$ and $\theta_i = -50^\circ$, this metasurface can realize anomalous refraction to $\theta_t = 0^\circ$ and specular reflection with power efficiencies of 14% and 82% respectively. The power scattered to unwanted directions are about 1.3% in total, indicating a low absorption loss of less than 3%. Fig. 6(b) shows the electric field magnitude distributions of the proposed metasurface upon incident Gaussian beams with $\theta_i = 50^\circ$ and $\theta_i = -50^\circ$ respectively. From Fig. 6(b) we can observe that the proposed metasurface achieves the required transmission and reflection characteristics.

TABLE I
GEOMETRICAL PARAMETERS AND S PARAMETERS OF THE UNIT CELLS

| Unit cell No. | | 1 | 2 |
|-----------------------------|------------------|--------|------|
| Geometrical parameters [mm] | L_{top} | 2.6 | 5.0 |
| | W_{top} | 0.5 | 0.5 |
| | L_{mid} | 2.6 | 1.4 |
| | W_{mid} | 1.0 | 0.5 |
| | L_{bot} | 2.6 | 5.0 |
| | W_{bot} | 0.5 | 1.0 |
| Transmission coefficient | Magnitude | 0.88 | 0.90 |
| | Phase difference | 178.4° | |
| Reflection coefficient | Magnitude | 0.43 | 0.42 |
| | Phase difference | 1.2° | |

We now find the waveguide height. The specular reflection mode of the proposed metasurface has a reflection phase of $\varphi_{r,MS} = 176^\circ$, then we can use (2) to find the required waveguide height, which is $h = 8.2$ mm.

Finally we construct the LWA using the proposed two-element metasurface. Fig. 7(a) shows one period of the proposed LWA and the simulation setup for extracting the LWA leakage factor. For wave travelling in either direction in the waveguide, the leakage factor of the proposed LWA can be extracted using the S parameters [1]

$$\alpha = \frac{1}{\Lambda_g} \text{Re} \left\{ \cosh^{-1} \left(\frac{1 - S_{11}S_{22} + S_{21}S_{12}}{2S_{21}} \right) \right\}. \quad (16)$$

Consider an LWA terminated with a matched load. The radiated power as a function of the antenna length L is

$$P_{\text{rad}} = 1 - \exp(-2\alpha L). \quad (17)$$

For a load-terminated LWA, the leakage factor, calculated using (16), is $\alpha = 0.011k_0$. Fig. 7(b) plots the percentage of the radiated power as a function of the antenna length. From Fig. 7(b), we can see that for an LWA terminated with a matched load, an antenna length of around $17\lambda_0$ is required to radiate 90% of the incident power. By placing a PEC at the waveguide end to reflect and radiate the wave, this antenna length can be dramatically reduced to less than $7\lambda_0$ while it still radiates 90%

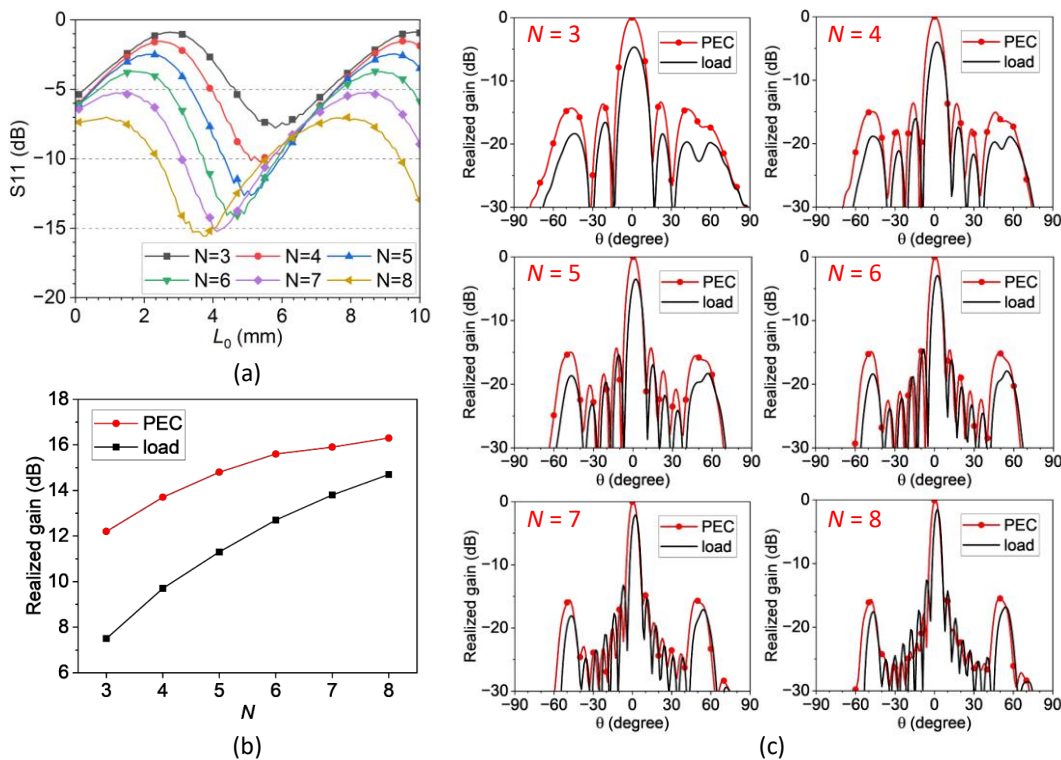


Fig. 8. (a) Reflection coefficient of the proposed LWA with different N as a function of L_0 . (b) Maximum realized gain of the LWAs terminated with PEC and load. (c) Radiation patterns of the LWAs terminated with PEC and load. For each N , the radiation patterns are normalized to the maximum realized gain of the proposed LWA (PEC-terminated).

of the incident power. (The directivity, though, will decrease with the reduction of the antenna length.) In general, the dramatic length reduction is due to (i) aperture reuse and (ii) the constructive interference of leaked waves. Fig. 7(c) plots the normalized electrical field intensity distributions of LWAs terminated with load and PEC, with antenna lengths of around $17\lambda_0$ and $7\lambda_0$ respectively. The sample points for field intensity distributions within the LWA, as found in full-wave simulation, are obtained by averaging the simulated field intensity within each metasurface period. For the LWA terminated with load, the simulated field intensity distribution agrees well with the calculated one. Compared to the LWA terminated with load, the field intensity distribution inside the LWA waveguide terminated with PEC is more uniform. This is due to the constructive interference of the two travelling waves, where the forward-travelling wave has higher intensity close to the waveguide feed, and the backward-travelling wave has higher intensity close to the waveguide termination. As a result, the more uniform field intensity distribution in the PEC-terminated LWA waveguide leads to a further gain enhancement. Fig. 7(d) shows the perspective view of the proposed LWA. The waveguide mid-section with the metasurface cover (with a length $L_{MS} = N\lambda_g$) is used to radiate power toward the broadside direction. The waveguide end-section without metasurface (with a length of L_0) is used to tune the phase of the reflected wave in the waveguide so that a constructive interference between the waves leaked from the forward and backward-travelling waves can be realized. The optimal L_0 depends on the interference between the metasurface and the travelling waves in the waveguide. Meanwhile, the impedance

mismatch at the connection point between the sections with and without metasurface may affect the wave interference. Therefore, a practical way to find the suitable L_0 is to sweep it and choose the one that minimize the return loss of the LWA.

Fig. 8 shows the simulated performance of the LWA. Fig. 8(a) plots the reflection coefficient magnitude of the proposed LWA with different N as a function of L_0 , from which we can find the optimal L_0 for each case. As we can see, the smallest $|S_{11}|$ decreases with increasing N . When N is larger than 4, the smallest $|S_{11}|$ is below -10 dB. For Figs. 8(b) and (c), we show the radiation and aperture efficiency enhancement of our proposed LWA by comparing our proposed (PEC-terminated) LWA with an LWA of the same length but terminated with a load at the waveguide end. Leakage in both LWAs are accomplished through the same metasurfaces with lengths $L_{MS} = N\lambda_g$. Fig. 8(b) compares the realized gain by both antennas for different values of N . We can observe a decreasing gain enhancement with increasing N , which is due to the decreasing reflected power at the PEC end of the LWA with an increasing antenna length. For the case with $N = 5$, we have $L_{MS} = 5\lambda_g = 70$ mm and $L_0 = 5$ mm, resulting a total antenna length of 75 mm, which is $7\lambda_0$. From Fig. 8(b) we can see, a $7\lambda_0$ long LWA terminated with a matched load only radiates 60% of the input power. In this case, our proposed design greatly increases the radiation efficiency, achieving a gain enhancement of 3.5 dB. Fig. 8(c) plots the radiation patterns of the LWAs on the yz plane ($\phi = 90^\circ$). The radiation patterns are normalized to the maximum realized gain of the proposed LWA. As expected, an increasing N will lead to a decreased gain enhancement and a narrower beam width. We can also see from Fig. 8(c) that, in all

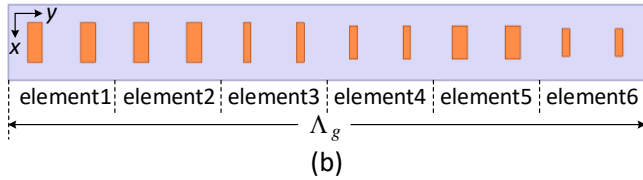
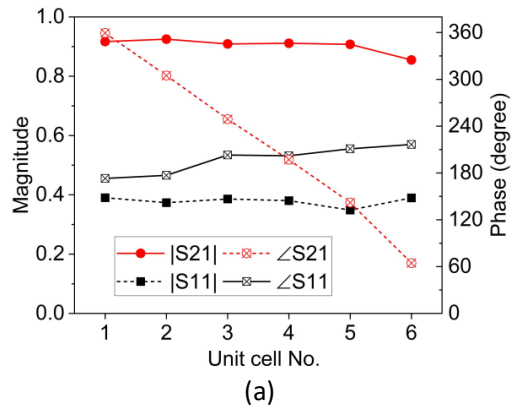


Fig. 9. (a) Magnitudes and phases of the transmission and reflection coefficients of the unit cells composing the proposed metasurface. (b) Top view of one period of the proposed six-element metasurface.

the cases, the sidelobe levels are lower than -14 dB, showing a good suppression of the spurious scattering achieved by the metasurface.

B. Tilted Radiation

As shown in (9) and (10), our proposed LWA can realize any tilted radiation angle with $11.5^\circ < |\theta_t| < 90^\circ$. Here we design an LWA to realize a tilted radiation with $\theta_t = 31^\circ$. We describe our LWA design following the design formulation in Section IIC. From Fig. 4 we can see that the desired radiation direction ($\theta_t = 31^\circ$) can be realized with a discrete metasurface with $M = 5$ or $M = 6$. Using (13) and (15) we can calculate the required incident angles and the element sizes of the two cases. For $M = 5$, they are $\theta_i = 59^\circ$ and $\frac{\Lambda_g}{M} = 6$ mm. For $M = 6$, they are $\theta_i = 50^\circ$ and $\frac{\Lambda_g}{M} = 7$ mm. We choose $M = 6$ in this design. The metasurface will have six elements per period, and each element will be composed of two identical unit cells. In this design, we use the same unit cell structure and size as shown in Fig. 5. Similarly, we tune the geometrical parameters of the rectangular strips to achieve unit cells with different transmission and reflection coefficients. We design six unit cells with similar reflection coefficients (magnitude and phase), while their transmission coefficients are similar in magnitude but with a phase gradient of 60° . Table II gives the geometrical parameters of the unit cells, whose magnitudes and phases of the transmission and reflection coefficients are plotted in Fig. 9(a). As we can see, for the transmission coefficients, the magnitudes are all around 0.9 while the phases show a gradient of around 60° . The reflection coefficients have similar magnitudes (around 0.4) and phases (about 30° deviation). Fig. 9(b) shows the top view of one period of the proposed six-element metasurface. Periodic simulation shows that, upon incidence with $\theta_i = 50^\circ$, this metasurface can realize

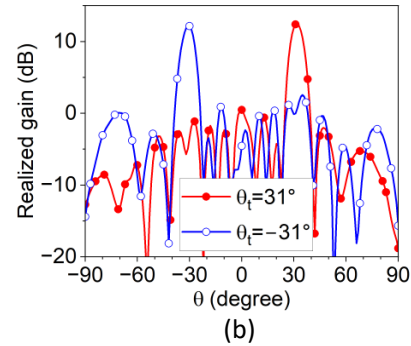
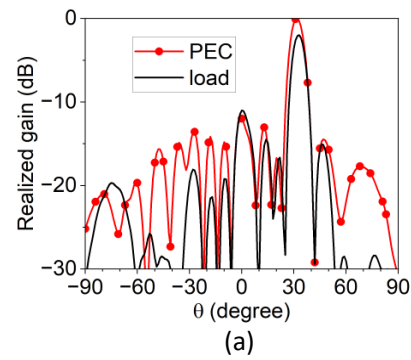


Fig. 10. (a) Radiation patterns of the LWAs (with $\theta_t = 31^\circ$) terminated with PEC and load. The radiation patterns are normalized to the maximum realized gain of the proposed LWA (PEC-terminated). (b) Radiation patterns of the proposed LWAs (PEC-terminated) with radiation angles of $\theta_t = 31^\circ$ and $\theta_t = -31^\circ$ respectively.

anomalous refraction to $\theta_t = 31^\circ$ and specular reflection with respective power efficiencies of 11% and 78%. Upon incidence with $\theta_i = -50^\circ$, this metasurface can realize anomalous refraction to $\theta_t = 31^\circ$ and specular reflection with respective power efficiencies of 6% and 78%. The incident angle of $\theta_i = -50^\circ$ requires a larger bending angle from the specular direction to the desired anomalous direction. Therefore, the spurious scattering in transmission slightly increases, leading to a decreased power efficiency in the desired diffraction mode.

TABLE II
GEOMETRICAL PARAMETERS OF THE UNIT CELLS

| Unit cell No. | 1 | 2 | 3 | 4 | 5 | 6 |
|----------------|-----|-----|-----|-----|-----|-----|
| L_{top} [mm] | 2.6 | 2.6 | 2.6 | 2.2 | 2.2 | 1.8 |
| W_{top} [mm] | 1.0 | 1.0 | 0.5 | 0.5 | 1.0 | 0.5 |
| L_{mid} [mm] | 2.6 | 2.2 | 3.4 | 4.6 | 1.0 | 1.0 |
| W_{mid} [mm] | 1.0 | 1.0 | 0.5 | 0.5 | 1.0 | 1.0 |
| L_{bot} [mm] | 3.0 | 3.0 | 3.0 | 3.0 | 3.8 | 4.2 |
| W_{bot} [mm] | 0.5 | 0.5 | 1.0 | 0.5 | 0.5 | 1.0 |

The specular reflection mode of the proposed metasurface has a reflection phase of $\varphi_{r,MS} = -141^\circ$. Using (2), we can find the required waveguide height, which is $h = 9.2$ mm. Then we construct the LWA using the proposed six-element metasurface. The leakage factor of the proposed LWA is $\alpha = 0.012k_0$, corresponding to a length of $15\lambda_0$ for an LWA with matched load to realize a 90% power radiation. Since the metasurface period ($\Lambda_g = 42$ mm) is about $4\lambda_0$, we design the LWA using a metasurface with two periods ($L_{MS} = 2\Lambda_g$). A

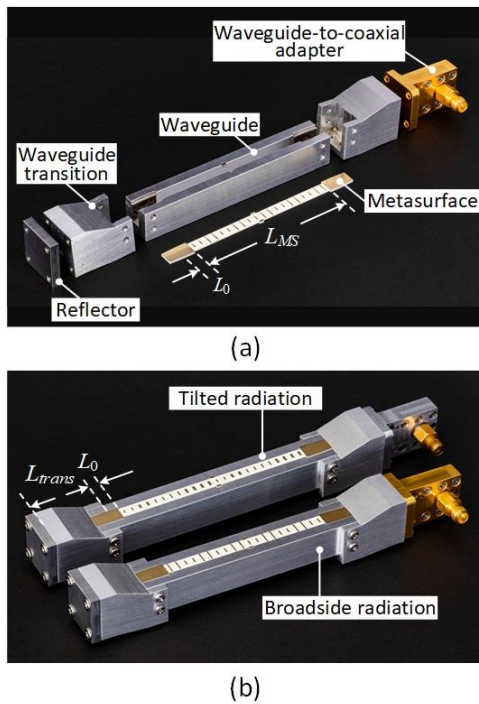


Fig. 11. Photos of the fabricated LWAs. (a) Unassembled LWA showing the fabricated parts. (b) The proposed LWAs.

waveguide section with no metasurface and a length of $L_0 = 5.0$ mm is added before the waveguide end to realize a constructive interference between the waves leaked from the forward and backward-travelling waves. Fig. 10(a) plots the radiation patterns of the LWAs terminated with PEC and load, normalized to the maximum realized gain of the proposed LWA. From Fig. 10(a) we can see, the proposed LWA realizes a tilted radiation to $\theta_t = 31^\circ$ with a sidelobe level below -10 dB. Besides, our proposed LWA achieves a 2.0 dB gain enhancement compared with the LWA terminated with a load.

By rotating the proposed metasurface by 180° around z-axis, the LWA can realize a tilted radiation angle of $\theta_t = -31^\circ$ (in the backward quadrant). Fig. 10(b) shows the radiation patterns of the LWAs (PEC-terminated) realizing radiation angles of $\theta_t = 31^\circ$ and $\theta_t = -31^\circ$ respectively. We can see that, for both LWAs, the sidelobe levels are below -10 dB, showing good radiation performance and suppressed scattering to spurious directions.

IV. FABRICATION AND EXPERIMENT

To validate the simulated results, we proceed to fabricate and measure the proposed LWAs. For the experiment, we design and fabricate a waveguide transition to realize an efficient conversion from the LWA waveguide to a standard size (8.64×4.32 mm²). To compare the performance of our proposed LWA with the one terminated with a load, a waveguide transition is also added at the end of the antenna. The length of the waveguide transition parts should be long enough to realize an efficient transition. Besides, to maintain the constructive interference between the waves leaked from the forward and backward-travelling waves, the length of the waveguide transitions should be an integral multiple of the half-guided

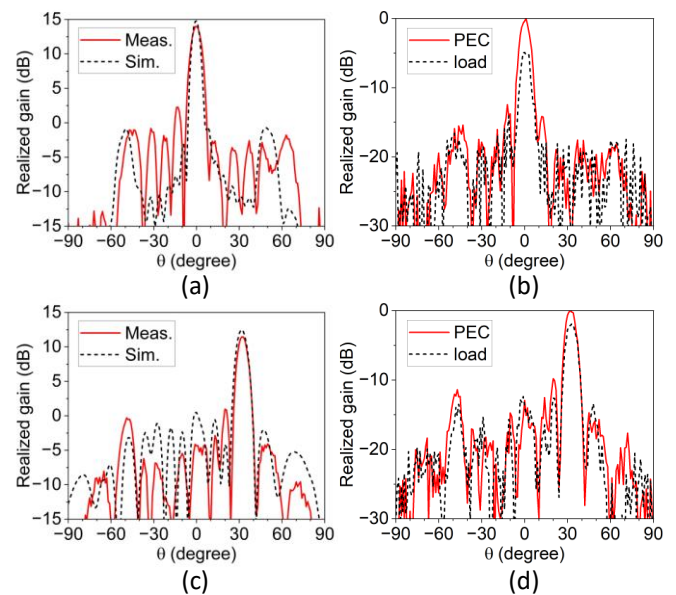


Fig. 12. (a) Measured and simulated radiation patterns of the proposed LWA realizing broadside radiation. (b) Comparison between the measured radiation patterns of the broadside radiation LWAs terminated with PEC and load. (c) Measured and simulated radiation patterns of the proposed LWA realizing tilted radiation with $\theta_t = 31^\circ$. (d) Comparison between the measured radiation patterns of the tilted radiation LWAs terminated with PEC and load.

wavelength ($\lambda_g = \frac{\lambda_0}{\sin \theta_t} = 14$ mm). Here the length of the waveguide transitions is designed to be 21 mm. Narrow grooves are fabricated in the waveguide for metasurface assembly. A metallic slab is used as a reflector at the end of the waveguide. The rectangular waveguide (without the top surface), waveguide transitions and the reflector are fabricated using aluminum alloy by computer numerical control (CNC) machining. The metasurfaces are fabricated by a standard PCB fabrication process.

Fig. 11(a) is a photo of the unassembled LWA, showing the fabricated parts. Fig. 11(b) shows a photo of the assembled LWAs. For the LWA realizing broadside radiation, we fabricate the LWA with a metasurface length of $L_{MS} = 5\lambda_g = 70$ mm. The LWA realizing tilted radiation has a metasurface length of $L_{MS} = 2\lambda_g = 84$ mm. In the experiment, waveguide-to-coaxial adapters (HD-260WCAV) are used for the antenna excitation and load. A vector network analyzer (R&S ZNA43-44) is used to measure the reflection coefficients of the proposed LWAs. Though the LWAs are both designed at 28 GHz, the fabrication errors introduce minor shifts in the working frequencies of the fabricated antennas. The measured working frequencies are 27.9 GHz and 27.6 GHz for the LWAs with broadside radiation and tilted radiation respectively. For the proposed LWA realizing broadside radiation, the measured S_{11} is -11.9 dB at 27.9 GHz. The measured radiation patterns are shown in Figs. 12(a) and (b). Fig. 12(a) shows the comparison between the measured and simulated radiation patterns of the proposed LWA, showing the achievement of broadside radiation. The measured and simulated maximum realized gains are 14.0 dB and 14.8 dB respectively. Fig. 12(b) compares the measured radiation patterns of the fabricated LWA terminated with PEC and load. The radiation patterns are

normalized to the maximum realized gain of the proposed LWA (PEC-terminated), showing a measured gain enhancement of 4.2 dB realized by the proposed LWA. For the proposed LWA realizing tilted radiation, the measured S_{11} is -14.1 dB at 27.6 GHz. Figs. 12 (c) plots the measured radiation pattern compared to the simulated one, showing the achievement of a tilted radiation to the desired direction. The measured and simulated maximum realized gains are 11.5 dB and 12.4 dB respectively. The sidelobe appearing at -50° in the measured radiation pattern is due to the specular transmission of the metasurface upon incidence with $\theta_i = -50^\circ$ (correspond to the backward-travelling wave in the waveguide). Fig. 12(d) compares the measured radiation patterns of the fabricated LWA terminated with PEC and load patterns of the maximum realized gain of the PEC-terminated LWA). From Fig. 12(d) we can observe a measured gain enhancement of 1.9 dB realized by the proposed LWA. For both LWAs, the drop in the measured maximum realized gain is caused by fabrication errors and the working frequency shifts. Nevertheless, the measured gain decreases by less than 1 dB for both LWAs, showing good agreement between the measurement and simulation results. Besides, for both LWAs, the sidelobe levels of the measured radiation patterns are below -10 dB, showing that the metasurfaces achieve good suppression of the spurious scatterings.

V. DISCUSSION ON BANDWIDTH

The proposed method is designed to work for a single frequency. A change in the frequency will affect the LWA performance in two aspects. Firstly, the frequency change will change the incident angle of the travelling waves in the rectangular waveguide, leading to a discrepancy between the refraction angles of the waves leaked from the forward and backward travelling waves. Secondly, the frequency change will change the interference between the forward and backward travelling waves for an LWA with a determined length, which may lead to radiation efficiency degradation. Therefore, the proposed LWAs feature narrow bandwidth performance. Fig. 13 shows the simulated realized gains of the proposed LWAs at the designed radiation direction, showing 3-dB gain bandwidths of 3.6% and 2.2% for the broadside radiation LWA and the tilted (31°) radiation LWA respectively. Fig. 14 plots the radiation patterns of the proposed LWAs at different frequencies. From Fig. 14 we can see, for both LWAs, when the frequency is deviated from the design frequency, the maximum realized gain drops while the sidelobes increase.

Nevertheless, the bandwidths of the proposed LWAs are limited by the single beam radiation functionality. The proposed method of designing a discrete metasurface in the LWA can be used to realize some other functionalities with broader bandwidth. For example, a dual-beam LWA can be designed to realize different radiation angles for the forward and backward travelling waves. In principle, the bandwidth of this dual-band LWA can be made comparable to the bandwidth of the anomalous refraction discrete metasurface, which we have shown in a previous work to be relatively large [34].

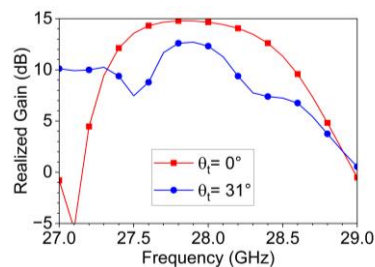


Fig. 13. Simulated realized gains of the proposed LWAs at the designed radiation direction.

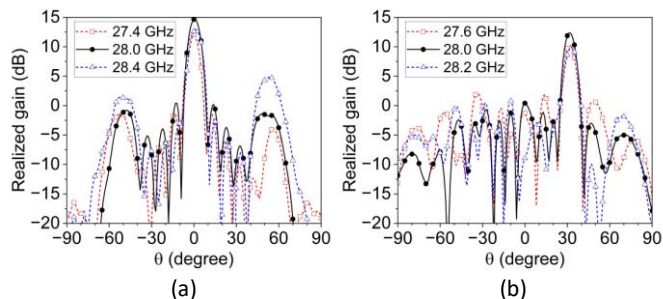


Fig. 14. Simulated radiation patterns of (a) the proposed LWA realizing broadside radiation and (b) the proposed LWA realizing tilted radiation with $\theta_t = 31^\circ$ at different frequencies.

VI. CONCLUSION

We have proposed a novel concept of LWAs based on discrete metasurfaces. Compared to a traditional LWA with matched termination at the end of the waveguide, the proposed LWA realizes gain enhancement by reflecting and radiating the remaining power reaching the end of the waveguide, in such a way that the radiation direction and relative phase are aligned for the waves leaked from the forward and backward-travelling waves. Hence the two wave components constructively interfere to increase the antenna gain. We show in this work that the aforementioned concept can be realized by an LWA based on a discrete metasurface, which is designed to contribute differing transverse momenta to the forward and backward-travelling waves in the waveguide. The metasurface is placed as the top surface of the LWA to generate the required radiation; a flat metallic reflector is aptly positioned at the end of the waveguide to reflect the guided wave and achieve the required phase alignment. We have designed two LWAs at 28 GHz to demonstrate the concept: a two-element metasurface LWA for broadside radiation and a six-element metasurface LWA for tilted radiation with $\theta_t = 31^\circ$. Simulation and experimental results agree, and show that gain enhancements of 4.2 dB (broadside LWA) and 1.9 dB (31° -radiating LWA) have been achieved, compared to LWAs of similar designs with a matched termination. The proposed discrete metasurface-based LWAs achieve improved radiation efficiencies and reduced antenna lengths, and can find potential applications in various communication systems.

REFERENCES

- [1] D. R. Jackson, and A. A. Oliner, "Leaky-wave antennas" in Modern Antenna Handbook, New York: Wiley, 2008.

- [2] J. L. Volakis, *Antenna engineering handbook*: McGraw-Hill Education, 2007.
- [3] D. R. Jackson, C. Caloz, and T. Itoh, "Leaky-wave antennas," *Proc. IEEE*, vol. 100, no. 7, pp. 2194-2206, 2012.
- [4] A. Sutunjo, M. Okoniewski, and R. H. Johnston, "Radiation from fast and slow traveling waves," *IEEE Antennas and Propagation Magazine*, vol. 50, no. 4, pp. 175-181, 2008.
- [5] R. Elliott, "An improved design procedure for small arrays of shunt slots," *IEEE Transactions on Antennas and Propagation*, vol. 31, no. 1, pp. 48-53, 1983.
- [6] J. C. Coetzee, J. Joubert, and D. A. McNamara, "Off-center-frequency analysis of a complete planar slotted-waveguide array consisting of subarrays," *IEEE Transactions on Antennas and Propagation*, vol. 48, no. 11, pp. 1746-1755, 2000.
- [7] H. V. Nguyen, S. Abielmona, and C. Caloz, "Highly efficient leaky-wave antenna array using a power-recycling series feeding network," *IEEE Antennas Wirel. Propag. Lett.*, vol. 8, pp. 441-444, 2009.
- [8] H. V. Nguyen, A. Parsa, and C. Caloz, "Power-recycling feedback system for maximization of leaky-wave antennas' radiation efficiency," *IEEE Trans. Microw. Theory Techn.*, vol. 58, no. 7, pp. 1641-1650, 2010.
- [9] B. B. Tierney, and A. Grbic, "Arbitrary beam shaping using 1-D impedance surfaces supporting leaky waves," *IEEE Trans. Antennas Propag.*, vol. 63, no. 6, pp. 2439-2448, 2015.
- [10] W. Fuscaldo, A. Galli, and D. R. Jackson, "Optimization of the radiating features of 1-D unidirectional leaky-wave antennas," *IEEE Trans. Antennas Propag.*, vol. 70, no. 1, pp. 111-125, 2021.
- [11] W. Fuscaldo, A. Galli, and D. R. Jackson, "Optimization of 1-D unidirectional leaky-wave antennas based on partially reflecting surfaces," *IEEE Trans. Antennas Propag.*, vol. 70, no. 9, pp. 7853-7868, 2022.
- [12] C. L. Holloway, E. F. Kuester, J. A. Gordon *et al.*, "An overview of the theory and applications of metasurfaces: The two-dimensional equivalents of metamaterials," *IEEE Antenn. Propag. Mag.*, vol. 54, no. 2, pp. 10-35, 2012.
- [13] E. F. Kuester, M. A. Mohamed, M. Piket-May *et al.*, "Averaged transition conditions for electromagnetic fields at a metafilm," *IEEE Trans. Antennas Propag.*, vol. 51, no. 10, pp. 2641-2651, 2003.
- [14] T. R. Cameron, and G. V. Eleftheriades, "Experimental validation of a wideband metasurface for wide-angle scanning leaky-wave antennas," *IEEE Trans. Antennas Propag.*, vol. 65, no. 10, pp. 5245-5256, 2017.
- [15] B. H. Fong, J. S. Colburn, J. J. Ottusch *et al.*, "Scalar and tensor holographic artificial impedance surfaces," *IEEE Trans. Antennas Propag.*, vol. 58, no. 10, pp. 3212-3221, 2010.
- [16] D.-H. Kwon, "Modulated reactance surfaces for leaky-wave radiation based on complete aperture field synthesis," *IEEE Trans. Antennas Propag.*, vol. 68, no. 7, pp. 5463-5477, 2020.
- [17] D.-H. Kwon, "Modulated scalar reactance surfaces for endfire radiation pattern synthesis," *IEEE Trans. Antennas Propag.*, vol. 70, no. 1, pp. 440-450, 2021.
- [18] H. Lee, and D.-H. Kwon, "Printed Metasurface Leaky-Wave Antennas Based on Penetrable Aperture Field Synthesis," *IEEE Trans. Antennas Propag.*, 2023.
- [19] G. Minatti, M. Faenzi, E. Martini *et al.*, "Modulated metasurface antennas for space: Synthesis, analysis and realizations," *IEEE Trans. Antennas Propag.*, vol. 63, no. 4, pp. 1288-1300, 2014.
- [20] A. M. Patel, and A. Grbic, "A printed leaky-wave antenna based on a sinusoidally-modulated reactance surface," *IEEE Trans. Antennas Propag.*, vol. 59, no. 6, pp. 2087-2096, 2011.
- [21] S. Sun, Q. He, S. Xiao *et al.*, "Gradient-index meta-surfaces as a bridge linking propagating waves and surface waves," *Nat. Mater.*, vol. 11, no. 5, pp. 426-431, 2012.
- [22] G. Xu, A. Overvig, Y. Kasahara *et al.*, "Arbitrary aperture synthesis with nonlocal leaky-wave metasurface antennas," *Nat. Commun.*, vol. 14, no. 1, pp. 4380, 2023.
- [23] C. Pfeiffer, and A. Grbic, "Metamaterial Huygens' surfaces: tailoring wave fronts with reflectionless sheets," *Phys. Rev. Lett.*, vol. 110, no. 19, pp. 197401, May, 2013.
- [24] M. Selvanayagam, and G. V. Eleftheriades, "Discontinuous electromagnetic fields using orthogonal electric and magnetic currents for wavefront manipulation," *Opt. Express*, vol. 21, no. 12, pp. 14409-14429, Jun., 2013.
- [25] E. Abdo-Sánchez, M. Chen, A. Epstein *et al.*, "Experimental verification of a leaky-wave antenna based on a bianisotropic Huygens' metasurface," in *Proc. Eur. Conf. Antennas Propag. (EUCAP)*, 2019, pp. 1-5.
- [26] E. Abdo-Sánchez, M. Chen, A. Epstein *et al.*, "A Leaky-Wave Antenna With Controlled Radiation Using a Bianisotropic Huygens' Metasurface," *IEEE Trans. Antennas Propag.*, vol. 67, no. 1, pp. 108-120, 2019.
- [27] E. Abdo-Sánchez, A. Epstein, and G. V. Eleftheriades, "Bianisotropic Huygens' metasurface leaky-wave antenna with flexible design parameters," in *Proc. Eur. Conf. Antennas Propag. (EUCAP)*, 2017, pp. 3315-3318.
- [28] P. Mateos-Ruiz, V. K. Killamsetty, A. Epstein *et al.*, "Physical Implementation of Leaky-Wave Antenna with Engineered Aperture Distribution Based on Bianisotropic Huygens Metasurfaces," in *Proc. Eur. Conf. Antennas Propag. (EUCAP)*, 2023, pp. 1-5.
- [29] B. B. Tierney, and A. Grbic, "Controlling leaky waves with 1-D cascaded metasurfaces," *IEEE Trans. Antennas Propag.*, vol. 66, no. 4, pp. 2143-2146, 2018.
- [30] P. Mateos-Ruiz, V. K. Killamsetty, A. Epstein *et al.*, "Arbitrary and Rigorous Aperture Illumination Synthesis in Huygens' Metasurface-Based Leaky-Wave Antennas," *IEEE Trans. Antennas Propag.*, 2025.
- [31] E. Abdo-Sánchez, A. Epstein, and G. V. Eleftheriades, "Reconfigurability Mechanisms With Scanning Rate Control for Omega-Bianisotropic Huygens' Metasurface Leaky-Wave Antennas," *IEEE Access*, vol. 7, pp. 168247-168260, 2019.
- [32] M. Kim, and G. V. Eleftheriades, "Reconfigurable leaky-wave antennas with independent control of the leakage constant and radiation angle," in *Proc. Eur. Conf. Antennas Propag. (EUCAP)*, 2020, pp. 1-5.
- [33] M. Kim, and G. V. Eleftheriades, "Guided-Wave-Excited Binary Huygens' Metasurfaces for Dynamic Radiated-Beam Shaping with Independent Gain and Scan-Angle Control," *Phys. Rev. Appl.*, vol. 15, no. 5, 2021.
- [34] C. Qi, and A. M. H. Wong, "Discrete Huygens' metasurface: Realizing anomalous refraction and diffraction mode circulation with a robust, broadband and simple design," *IEEE Trans. Antennas Propag.*, vol. 70, no. 8, pp. 7300-7305, 2022.
- [35] C. Qi, and A. M. H. Wong, "Aggressively Discretized Huygens' Metasurface: Realizing Efficient Anomalous Refraction with a Simple Design," in *International Congress on Artificial Materials for Novel Wave Phenomena (Metamaterials)*, 2021, pp. 350-352.
- [36] C. Qi, and A. M. H. Wong, "Broadband efficient anomalous reflection using an aggressively discretized metasurface," *Opt. Express*, vol. 30, no. 9, pp. 15735-15746, Apr 25, 2022.
- [37] A. M. H. Wong, P. Christian, and G. V. Eleftheriades, "Binary Huygens' metasurfaces: experimental demonstration of simple and efficient near-grazing retroreflectors for TE and TM polarizations," *IEEE Trans. Antennas Propag.*, vol. 66, no. 6, pp. 2892-2903, Jun., 2018.
- [38] A. M. H. Wong, and G. V. Eleftheriades, "Perfect anomalous reflection with a bipartite Huygens' metasurface," *Phys. Rev. X*, vol. 8, no. 1, pp. 011036, Feb., 2018.
- [39] C. Qi, and A. M. H. Wong, "A coarsely discretized Huygens' metasurface for anomalous transmission," in *Proc. IEEE Asia-Pacific Microw. Conf. (APMC)*, 2019, pp. 935-937.
- [40] Y. Ra'adi, D. L. Sounas, and A. Alù, "Metagratings: Beyond the limits of graded metasurfaces for wave front control," *Phys. Rev. Lett.*, vol. 119, no. 6, pp. 067404, Aug., 2017.
- [41] D. Sell, J. Yang, S. Doshay *et al.*, "Large-angle, multifunctional metagratings based on freeform multimode geometries," *Nano Lett.*, vol. 17, no. 6, pp. 3752-3757, May, 2017.
- [42] V. Popov, F. Boust, and S. N. Burokur, "Controlling diffraction patterns with metagratings," *Phys. Rev. Appl.*, vol. 10, no. 1, pp. 011002, Jul., 2018.
- [43] O. Rabinovich, and A. Epstein, "Arbitrary diffraction engineering with multilayered multielement metagratings," *IEEE Trans. Antennas Propag.*, vol. 68, no. 3, pp. 1553-1568, Mar., 2019.
- [44] O. Rabinovich, and A. Epstein, "Analytical design of printed circuit board (PCB) metagratings for perfect anomalous reflection," *IEEE Trans. Antennas Propag.*, vol. 66, no. 8, pp. 4086-4095, Aug., 2018.
- [45] G. V. Trentini, "Partially reflecting sheet arrays," *IRE Trans. Antennas Propag.*, vol. 4, no. 4, pp. 666-671, 1956.

- [46] C. Qi, X. He, B. Ren, and A. M. H. Wong, "Broadband terahertz metalenses based on printed circuit board fabrication," *Adv. Opt. Mater.*, vol. 12, no. 11, pp. 2302459, 2024.